J of Nuclear Medicine Technology, first published online July 30, 2021 as doi:10.2967/jnmt.121.262462

Assessing the correlation between ^{68}Ga-PSMA-11 renal PET parameters and renal function tests

Jan-Henning Schierz[1], Ismet Sarikaya[2], Ahmed N. Albatineh[3], Ali Sarikaya[4]

[1]Municipal Hospital Dresden, Department of Radiology, Dresden, Germany

[2]Kuwait University Faculty of Medicine, Department of Nuclear Medicine, Kuwait

[3]Faculty of Medicine, Department of Community Medicine and Behavioral Sciences, Kuwait University, Kuwait

[4]Trakya university Faculty of Medicine, Department of Nuclear Medicine, Turkey

Correspondence Address:

Ismet Sarikaya, MD, ABNM, Professor (Turkey)
Assoc. Professor
Department of Nuclear Medicine
Faculty of Medicine, Kuwait University
PO Box 24923
Safat, Kuwait 13110
Phone: (965) 25319592 / 6414
Fax: (965) 25338936
Email: isarikaya99@yahoo.com

Running title: PSMA renal PET and kidney function tests

Abstract

Aim: ^{68}Ga -PSMA ligands are used for prostate cancer but also show high renal cortical uptake. In this study, we aimed to assess if there is any correlation between renal PSMA PET parameters and renal function tests using the images of prostate cancer patients.

Methods: ^{68}Ga-PSMA-11 PET/CT images of the patients with prostate cancer were retrospectively evaluated. The following PET parameters were obtained: SUV_{max}, SUV_{mean}, SUL_{max}, SUL_{mean}, volume, TLG_{SUL} and counts of both kidneys as well as SUV_{mean} of liver, blood pool and spleen. Total TLG_{SUL}, total volume, kidney to liver and kidney to blood pool ratios were calculated. Patient's creatinine values were obtained and GFR was calculated using the MDRD formula. Statistical analysis was performed to understand if there is a correlation between above parameters and renal function tests.

Results: Twenty five patients were included in this study. GFR was significantly/positively correlated and creatinine was significantly/negatively correlated with renal SUV/liver SUV and renal SUV/blood pool SUV ratios. GFR was marginally positively correlated with renal SUL_{mean} and creatinine was marginally negatively correlated with total TLG_{SUL}. Total renal parenchymal volume was significantly and directly (positively) associated with GFR and significantly and inversely (negatively) associated with creatinine.

Conclusion: Renal ^{68}Ga-PSMA uptake appears to be correlated with renal function tests. Our method of measuring approximate renal parenchymal volume on PET image appears to be reliable.

Key words: PET/CT, Ga-68 PSMA-11, kidney, renal function

Introduction

PSMA, also known as glutamate carboxypeptidase II or folate hydrolase, is a Type II transmembrane protein which is mainly found in prostate tissue. It is overexpressed in prostate cancer and various other malignancies and also in extraprostatic normal tissues with highest expression in the kidneys and salivary glands (*1-3*). In immunohistochemical analysis, detectable PSMA levels were identified in the brush borders and apical cytoplasm of a subset of proximal renal tubules where it is responsible for the reuptake of folates via epithelial brush cells (*1,4*). Renal folate reabsorption seems to be primarily mediated by the glycosylphosphatidylinositol-(GPI) anchored protein folate receptor α (FRα), which is highly expressed at the brush-border membrane of proximal tubule cells (1,4-6).

^{68}Ga‑prostate specific membrane antigen (^{68}Ga-PSMA) ligands or inhibitors are novel positron emission tomography (PET) radiotracers to image prostate cancer and its metastases (7, 8). Recently, ^{68}Ga-PSMA-11 has been approved by FDA for prostate cancer imaging and other PSMA ligands (^{68}Ga and ^{18}F) are currently being evaluated in Europe for approval by the EMEA (9). Radiolabeled PSMA ligands with ^{177}Lu and ^{225}Ac are also used to treat prostate cancer metastases with increasing success (10, 11). Studies have reported no significant effect on renal function although therapeutic radiolabeled PSMA ligands show high renal uptake and excretion (12, 13).

In various articles Sarikaya et al. reported that ^{68}Ga-PSMA-11 shows excellent uptake and distribution in the renal parenchyma and demonstrates defects caused by various size of simple cortical cysts (14-16). In a case with chronic pyelonephritis, image resolution of renal PSMA PET as part of a prospective study in adults was superior to DMSA scan (17).

DMSA is the current gold standard for renal cortical imaging but there is a shortage of this tracer in various countries, including the US and there is a need for alternative radiotracers to image renal cortex (18).

Renal uptake of ^{99mTc}-DMSA has been shown to correlate well with the effective renal plasma flow (ERPF), glomerular filtration rate (GFR) and creatinine clearance (19-23).

In this study we wanted to determine if there is a correlation between renal PSMA PET parameters and renal function tests. Our aim was to understand if (1) PSMA PET could be suitable for renal cortical imaging and (2) if PSMA uptake parameters could be used to assess or estimate renal function in patients treated with radiolabeled PSMA ligands.

Material and Methods

We retrospectively analyzed the ^{68}Ga-PSMA-11 PET/CT images of prostate cancer patients who had renal function tests (creatinine) within 14 days of imaging. All images were obtained in the Nuclear Medicine Department at Dresden Municipal Hospital, Germany.

Tracer production and image acquisition

Radiolabeling of ^{68}Ga-PSMA-11 was carried out with an automated module (Scintomics GRP, Germany) as described previously (24).

Whole body PSMA PET/CT images were obtained using a Siemens Biograph 16 PET/CT camera (Siemens Healthineers, Erlangen, Germany) approximately 60 min after intravenous injection of 100-150 MBq (2.7 - 4.0 mCi) of ^{68}Ga‑PSMA-11.

Before PET image acquisition, a low-dose, unenhanced CT from vertex to mid-thigh was obtained for attenuation correction, anatomic localization and gross anatomical correlation purposes. CT parameters included 16 mAs, 120 KV, 0.8 pitch, 0.5, 20x0.6mm collimation and 5 mm reconstructed slice thickness.

PET acquisition time was 3 min/bed. The images were corrected for attenuation on the basis of the CT data and reconstructed using an iterative algorithm (Siemens TrueX) and reformatted as well as fused online into transaxial, coronal**,** and sagittal views with Syngo Via MM Oncology VB40 (Siemens Healthineers, Erlangen, Germany).

PET image analysis

Due to intense activity in the kidneys, PET images were analyzed in low intensity settings to better see the renal cortical uptake and distribution and accurately place VOI without including pelvicalyceal activity. For each kidney the three orthogonal planes on CT and PET were adjusted to optimally draw an ovoid VOI around the respective kidney and exclude possible extrarenal or calyceal activity (Figure 1). Following the plane alignment the VOI was drawn around the kidney and fitted around the external border of the cortex. To exclude the renal pelvis we used a lower limit of $SUV_{max} \geq 10$ for an automatically created isocontour VOI (Figure 1). Another attempt using a lower limit of 10% of SUV_{max} yielded suboptimal results as often a larger part of the renal pelvis was included in the isocontour VOI when the kidney SUV_{max} was too low.

Measured values:

PET parameters (SUV_{max}, SUV_{mean}, volume, total counts) of each kidney were determined on AC PET images. SUV_{mean} of the liver, spleen and blood pool were also obtained with standard VOIs provided by the software (Figure 2).

Calculated values:

From the measured values SUL_{max}, SUL_{mean} and TLG_{SUL} were calculated for each kidney using the lean body mass that was determined utilizing the Janmahasatian formula to take the highly variant patients BMI (ranging from 22.7 to 37.6) into account (25).

Finally we calculated the mean renal SUV_{max}, SUL_{max}, SUV_{mean} and SUL_{mean} (arithmetic mean of right and left kidney) as well as kidney/liver, and kidney/blood pool ratios using mean renal SUV_{max} and SUV_{mean} .

We also calculated total counts, total TLG and total volumes of both kidneys (sum of values of both kidneys).

GFR was calculated using the MDRD formula (26).

Statistical analysis

Statistical analysis was conducted using SPSS statistical software (27). Data were checked and cleaned for any abnormalities and coded accordingly. Simple descriptive statistics including mean, standard deviation (SD), min and max were calculated.

The most common procedure to get a point estimate for strength of linear relationship between two continuous variables is to use Pearson correlation coefficient – provided that the variables follow normal distributions. In the presence of outliers or when the data is not normally distributed but can be ranked, the Spearman rank correlation is the best option.

To get a confidence interval estimate of the correlation coefficient in case of non-normal data or with small sample size, and to diminish the effects of outliers, the bootstrap procedure which is a computer-intensive resampling technique can be implemented to produce a confidence interval estimate for the correlation coefficient.

In this analysis, since some of the covariates were not normally distributed and there were some outliers, we used Spearman rank correlation coefficient to estimate the strength of linear relationship and the bias-corrected and accelerated bootstrap method based on 2000 re-samplings to produce 95% confidence intervals for the correlation coefficient.

In order to find the most parsimonious multiple linear regression model with covariates that are significantly associated with GFR and creatinine, a stepwise regression method with backward substitution was implemented.

The final multiple linear regression model with significant covariates and their probability value (PV), and 95% confidence intervals for the estimated effect sizes were estimated. Outcomes were tested for normality. The linearity assumption between the outcome and the covariates was checked by Spearman rank correlation coefficient.

The final models were tested for significance, residuals were tested for normality, and multicollinearity was checked for all covariates to ensure that no two covariates that are highly correlated were included in the final model. All tests were two-tailed and probability value (PV) < 0.05 was considered statistically significant.

Results

From 2018 to 2020 we included 25 male patients in this study, mean (SD) age of 71.6 (9.84) years and a mean (SD) BMI of 28.7 (4.0). Patient characteristics, GFR and creatinine values are shown in Table 1. Two patients were excluded due to high calyceal activity. All patients received diuretic (Lasix) injection. None of the patients had pyelonephritis or hydronephrosis. Mean interval between injection and imaging was 64 min and range 60-70 min.

Isocontour VOIs using a lower threshold of SUV_{max}>10 made it possible to quickly estimate the approximate renal parenchymal volume (Figure 1), provided that there was no residual tracer in the renal pelvis, which would overestimate the renal counts, SUVs and renal volumes (Figure 3). In most of the cases kidneys had symmetrical appearance and uptake. Seven patients, however, showed either large cysts or defects and two of those showed remarkable asymmetry in measured volume and TLG but not in uptake (SUV_{max}, SUV_{mean}).

(Figure 4).

Table 2 shows mean SUV_{max}, SUV_{mean}, SUL_{max}, SUL_{mean} (arithmetic mean of right and left kidney), total volume and total TLG of the kidneys and SUV_{mean} of liver, blood pool and spleen.

The estimated Spearman rank correlation coefficient between GFR and Creatinine with several covariates along with their PV and 95% confidence interval estimate were presented in Table 3. GFR was significantly and positively correlated with renal to liver and renal to blood pool ratios (mean renal SUV_{max} to liver ratio, mean renal SUV_{max} to blood pool ratio, mean renal SUV_{mean} to liver ratio, mean renal SUV_{mean} to blood pool ratio) and age, while it was marginally significantly and positively correlated with mean SUL_{mean}. GFR was significantly and negatively correlated with SUV_{mean} blood pool.

On the other hand, creatinine was significantly and negatively correlated with renal SUV to liver and renal SUV to blood pool ratios (mean renal SUV_{max} to liver ratio, mean renal SUV_{max} to blood pool ratio, mean renal SUV_{mean} to liver ratio, mean renal SUV_{mean} to blood pool ratio), and age while it was marginally significantly and negatively correlated with total TLG_{SUL}. It was marginally positively correlated with age and marginally negatively correlated with SUV_{mean} blood pool.

In two stepwise regression models for GFR and creatinine as outcomes, total renal parenchymal volume was significantly and directly (positively) associated with GFR (β=0.12 (PV=0.008) (95% CI: 0.035, 0.205) and significantly and inversely (negatively) associated with creatinine (β= - 0.113 (PV=0.009) (95% CI: -0.195, -0.032).

Discussion

^{99m}Tc-DMSA is a widely used radiotracer to image renal cortex. The scan is mainly used to detect renal parenchymal defects caused by acute pyelonephritis or renal sequelae (scarring) 6

months after acute infection (28-30). It also helps detect renal abnormalities. The uptake quantification (percent contribution to total renal function or parenchyma) is used to decide if surgery is necessary and to assess the split renal function before surgery.

Currently there is a shortage of DMSA cold kit in various countries, including US (*18*). ^{99m}Tc-glucoheptonate is another radiotracer used to image the renal cortex when ^{99m}Tc-DMSA is not available but it is only partially concentrated in the kidneys and then excreted in the urine (30). ^{68}Ga-Alizarin Red S was studied in animals and humans as a renal cortical PET radiotracer in 1980s (31). Recently, MRI is gaining popularity in the diagnosis of pyelonephritis, however due to complex planning and scan times it is only used occasionally, i.e. in cases with pregnancy, where it has it's own drawbacks (32). In a recent meta-analysis study, Sarikaya et al. found overall equivalent sensitivity of MRI and DMSA scan in detecting parenchymal changes in pyelonephritis, particularly in scar detection (33). There is a need for PET radiotracers to image renal cortex with a higher resolution. Overall, PET scanners have higher spatial resolution than conventional gamma cameras and can detect smaller defects. On the other hand, new SPECT systems with cadmium zinc telluride (CZT) detectors have better resolution than conventional scanners with sodium iodide detectors (34). Recently, Sarikaya et al. reported that ^{68}Ga-PSMA PET provides excellent images of the renal cortex and shows defects caused by various size of cysts and provides higher resolution images as compared to DMSA scan (14-17).

Renal uptake of ^{99m}Tc-DMSA through planar and SPECT imaging in human and animals has been shown to correlate well with renal function tests, such as ERPF, GFR and creatinine clearance (19-23). Because of high renal cortical parenchymal uptake and excellent distribution with ^{68}Ga-PSMA, in the current study we wanted to determine if PSMA uptake is correlated with renal function tests. We found significant and positive correlation between GFR and renal SUV to

reference region ratios (liver and blood pool), and a marginal positive correlation with renal SUL_{mean}. Our statistical analysis also found a significant and negative correlation between creatinine and renal SUV to reference region ratios, and marginal correlation with renal sum TLG_{SUL}. As the SUVs are affected by body weight and various other factors, we used renal SUV to reference region ratios and also lean body mass corrected SUVs (SUL). Blood pool SUV was negatively correlated with GFR and positively correlated with creatinine as expected. Age was also negatively correlated with GFR and positively correlated with creatinine as expected. In two stepwise regression models total renal parenchymal volume was significantly and directly (positively) associated with GFR and significantly and inversely (negatively) associated with creatinine as expected. With aging kidney volumes reduces (35). Our method of measuring approximate renal parenchymal volume on PET image appears to be reliable. Other studies tried to correlate CT kidney volume with renal function but only found weak or moderate correlations in selected patient populations (36).

As radiolabeled PSMA ligands show high renal parenchymal uptake and renal excretion, studies have assessed renal function after ^{177}Lu-PSMA ligand treatments in metastatic prostate cancer patients. Studies have reported low renal toxicity in castrate-resistant metastatic prostate cancer treated with ^{177}Lu-PSMA-617 (12,13). However, it would be interesting to study larger number of patients who underwent ^{177}Lu-PSMA-therapy and correlate the renal function with the renal PSMA uptake parameters as we did in the current study. In animal models, DMSA uptake correlated with renal function loss in patients receiving chemotherapy (37). In a recent study, PSMA PET quantification of split renal function was compared to MAG3 scintigraphy which showed significant correlation between two methods (38).

The limitation of our study includes relatively small number of patients and having no

patients with GFR below 50, thus only measuring GFR in or just below the normal range for ages. Further work on mechanism and physiologic meaning of ^{68}Ga-PSMA-11 renal cortical uptake is also required.

Conclusion:

^{68}Ga-PSMA-11 renal cortical uptake correlates with renal function tests, such as GFR and creatinine. Our method of measuring approximate renal parenchymal volume on PET image appears to be reliable.

Disclosure

No potential conflict of interest relevant to this article was reported.

References

1. Silver DA, Pellicer I, Fair WR, Heston WD, Cordon-Cardo C. Prostate-specific membrane antigen expression in normal and malignant human tissues. *Clin Cancer Res.* 1997;3:81-5.
2. Mhawech-Fauceglia P, Zhang S, Terracciano L, et al. Prostate-specific membrane antigen (PSMA) protein expression in normal and neoplastic tissues and its sensitivity and specificity in prostate adenocarcinoma: an immunohistochemical study using mutiple tumour tissue microarray technique. *Histopathology*. 2007;50:472-83.
3. Cunha AC, Weigle B, Kiessling A, Bachmann M, Rieber EP. Tissue-specificity of prostate specific antigens: comparative analysis of transcript levels in prostate and non-prostatic tissues. *Cancer Lett.* 2006;236:229-38.
4. Baccala A, Sercia L, Li J, Heston W, Zhou M. Expression of prostate-specific membrane antigen in tumor-associated neovasculature of renal neoplasms. *Urology*. 2007; 70:385-90.
5. Samodelov SL, Gai Z, Kullak-Ublick GA, Visentin M. Renal Reabsorption of Folates: Pharmacological and Toxicological Snapshots. *Nutrients.* 2019;11:2353.
6. Glutamate Carboxypeptidase II. In: Rawlings ND, Salvesen G, eds. *Handbook of Proteolytic Enzymes*. London: Academic Press;2013:1620-1624.
7. Afshar‐Oromieh A, Avtzi E, Giesel FL, et al. The diagnostic value of PET/CT imaging with the (68)Ga‐labelled PSMA ligand HBED‐CC in the diagnosis of recurrent prostate cancer. *Eur J Nucl Med Mol Imaging.* 2015;42:197‐209.

8. Sonni I, Eiber M, Fendler WP, et al. Impact of (68)Ga-PSMA-11 PET/CT on staging and management of prostate cancer patients in various clinical settings: A Prospective single center study. *J Nucl Med.* 2020;61:1153-1160

9. Zippel C, Ronski SC, Bohnet-Joschko S, Giesel FL, Kopka K. Current Status of PSMA-Radiotracers for Prostate Cancer: Data Analysis of Prospective Trials Listed on ClinicalTrials.gov. *Pharmaceuticals*. 2020;13:12.

10. Violet J, Jackson P, Ferdinandus J, et al. Dosimetry of 177Lu-PSMA-617 in Metastatic Castration-Resistant Prostate Cancer: Correlations Between Pretherapeutic Imaging and Whole-Body Tumor Dosimetry with Treatment Outcomes. *J Nucl Med*. 2019;60:517-523.

11. Hofman MS, Emmett L, Sandhu S, et al. TheraP Trial Investigators and the Australian and New Zealand Urogenital and Prostate Cancer Trials Group. [177Lu]Lu-PSMA-617 versus cabazitaxel in patients with metastatic castration-resistant prostate cancer (TheraP): a randomised, open-label, phase 2 trial. *Lancet*. 2021;397:797-804. Epub 2021 Feb 11.

12. Yordanova A, Becker A, Eppard E, et al. The impact of repeated cycles of radioligand therapy using [177Lu]Lu-PSMA-617 on renal function in patients with hormone refractory metastatic prostate cancer. *Eur J Nucl Med Mol Imaging*. 2017;44:1473-1479.

13. Gallyamov M, Meyrick D, Barley J, Lenzo N. Renal outcomes of radioligand therapy: experience of 177lutetium-prostate-specific membrane antigen ligand therapy in metastatic castrate-resistant prostate cancer. *Clin Kidney J*. 2019;13:1049-1055.

14. Sarikaya I, Elgazzar AH, Alfeeli MA, Sarikaya A. Can gallium-68 prostate-specific membrane antigen ligand be a potential radiotracer for renal cortical positron emission tomography imaging? *World J Nucl Med*. 2018;17:126-129.
15. Sarikaya I, Sarikaya A. Current Status of Radionuclide Renal Cortical Imaging in Pyelonephritis. *J Nucl Med Technol*. 2019;47:309-312.
16. Sarikaya I. (68)Ga-PSMA Ligand as Potential (99m)Tc-DMSA Alternative. J Nucl Med. 2019;60:12N.
17. Sarikaya I, Alqallaf A, Sarikaya A. Renal Cortical 68Ga-PSMA-11 PET and 99mTc-DMSA Images. *J Nucl Med Technol*. 2021 Mar;49(1):30-33.
18. Lim R, Bar-Sever Z, Treves ST. Is availability of 99mTc-DMSA insufficient to meet clinical needs in the United States? A survey. J Nucl Med. 2019;60:14N–16N.
19. Taylor A Jr, Kipper M, Witztum K. Calculation of relative glomerular filtration rate and correlation with delayed technetium-99m DMSA imaging. *Clin Nucl Med*. 1986;11:28-31.
20. Taylor A: Quantitation of renal function with static imaging agents. *Semin Nucl Med* 1982;12:330-344
21. Kawamura J, Hosokawa S, Yoshida O, Fujita T, Ishii Y, Torizuka K. Validity of 99mTc dimercaptosuccinic acid renal uptake for an assessment for individual kidney function. *J Urol*. 1978;119:305-9.
22. Daly MJ, Jones W, Rudd TG, Tremann J. Differential renal function using technetium-99m dimercaptosuccinic acid (DMSA): in vitro correlation. *J Nucl Med*. 1979;20:63-6

23. Groshar D, Embon OM, Frenkel A, Front D. Renal function and technetium-99m-dimercaptosuccinic acid uptake in single kidneys: the value of in vivo SPECT quantitation. *J Nucl Med*. 1991;32:766-8.

24. Kleynhans J, Rubow S, le Roux J, Marjanovic-Painter B, Zeevaart JR, Ebenhan T. Production of [68 Ga]Ga-PSMA: Comparing a manual kit-based method with a module-based automated synthesis approach. *J Labelled Comp Radiopharm*. 2020;63:553-563.

25. Tahari AK, Chien D, Azadi JR, Wahl RL. Optimum lean body formulation for correction of standardized uptake value in PET imaging. *J Nucl Med*. 2014;55:1481-4

26. Levey AS, Bosch JP, Lewis JB, Greene T, Rogers N, Roth D. A more accurate method to estimate glomerular filtration rate from serum creatinine: a new prediction equation. Modification of Diet in Renal Disease Study Group. *Ann Intern Med*. 1999;130:461-70.

27. IBM Corp. Released 2020. IBM SPSS Statistics for Windows, Version 27.0. Armonk, NY: IBM Corp

28. Piepsz A, Colarinha P, Gordon I, et al. Paediatric Committee of the European Association of Nuclear Medicine. Guidelines for 99mTc-DMSA scintigraphy in children. *Eur J Nucl Med.* 2001;28:BP37-41.

29. Karmazyn BK, Alazraki AL, Anupindi SA, et al. Expert panel on pediatric imaging:, ACR appropriateness criteria(®) Urinary tract infection-Child. *J Am Coll Radiol*. 2017;14:S362-S371.

30. Mandell GA, Eggli DF, Gilday DL, et al. Procedure guideline for renal cortical scintigraphy in children. Society of Nuclear Medicine. *J Nucl Med*. 1997;38:1644-6.

31. Schuhmacher J, Maier-Borst W, Wellman HN. Liver and kidney imaging with Ga-68-labeled dihydroxyanthraquinones. *J Nucl Med*. 1980;21:983-7.

32. Mervak BM, Altun E, McGinty KA, Hyslop WB, Semelka RC, Burke LM. MRI in pregnancy: Indications and practical considerations. *J Magn Reson Imaging*. 2019;49:621-631.

33. Sarikaya I, Albatineh AN, Sarikaya A. 99mTc-dimercaptosuccinic acid scan versus MRI in pyelonephritis: a meta-analysis. *Nucl Med Commun*. 2020 Nov;41(11):1143-1152.

34. Daghighian F, Sumida R, Phelps ME. PET imaging: An overview and instrumentation. *J Nucl Med Technol*. 1990;18:5-13.

35. Gong IH, Hwang J, Choi DK, et al. Relationship Among Total Kidney Volume, Renal Function and Age. *The Journal of Urology* 2012;187, 344–349.

36. Matsuo M, Yamagishi F, Higuchi A. A Pilot Study of Prediction of Creatinine Clearance by Ellipsoid Volumetry of Kidney Using Noncontrast Computed Tomography. *JMA J*. 2019;2:60-66.

37. Demir F, Demir M, Aygun H. Evaluation of the protective effect of edaravone on doxorubicin nephrotoxicity by [99mTc]DMSA renal scintigraphy and biochemical methods. *Naunyn Schmiedebergs Arch Pharmacol*. 2020;393:1383-1390.

38. Rosar F, Pauly P, Ries M, et al. Determination of split renal function by PSMA imaging: comparison of 68Ga-PSMA-11 PET with 99mTc-MAG3 scintigraphy. *Am J Nucl Med Mol Imaging.* 2020;10:249-256.

Figure Legends

Figure-1

Example of VOI placement: An ovoid VOI is placed around the kidney (blue arrow). The software automatically traces the edge with a previous defined lower boundary of SUV_{max} =10, thus establishing an isocontour VOI with the whole cortical kidney volume (green arrow).

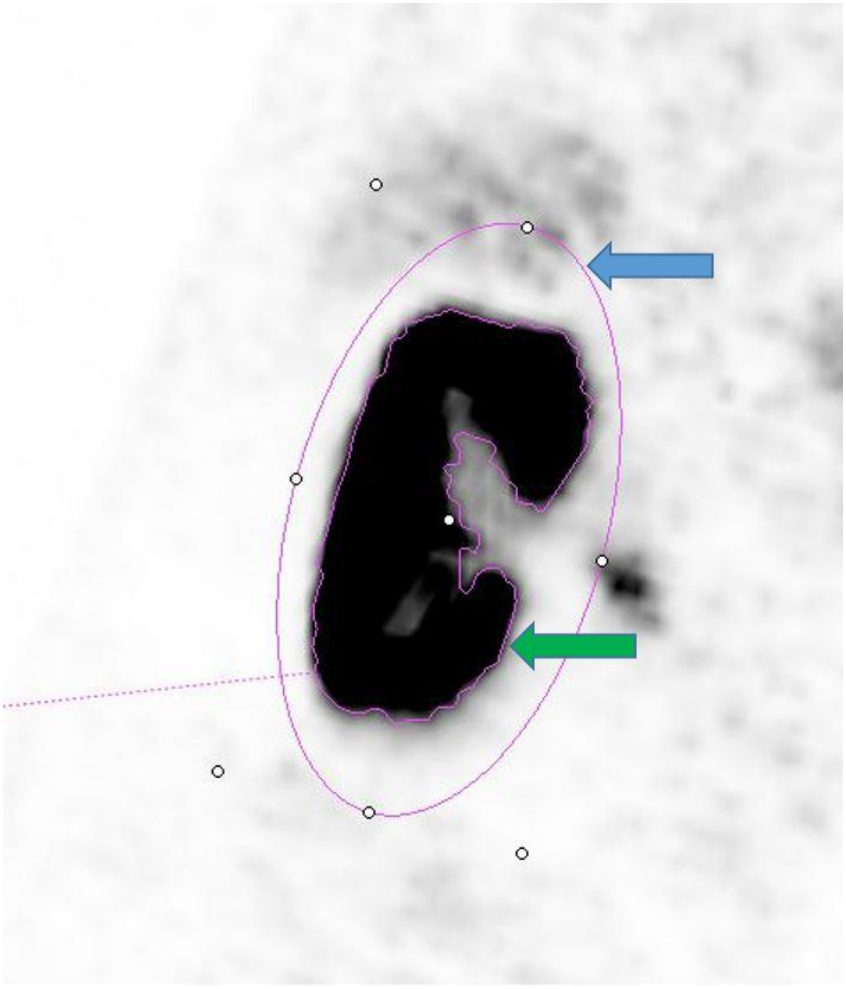

Figure 2

Example of VOI placement for liver (A), spleen (B) and blood pool (C). VOIs for liver and blood pool are drawn by the software while the splenic VOI had to be drawn manually.

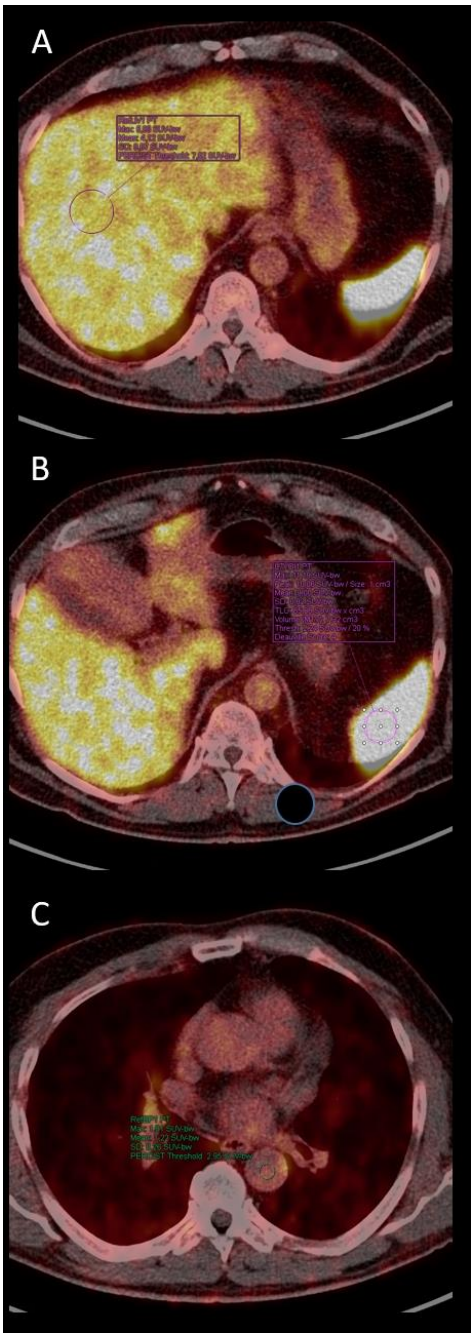

Figure-3

Example for an excluded patient: Because of a large portion of calyceal tracer (red circle), the patient was omitted from measurement as the software would add this area, falsifying the measured values.

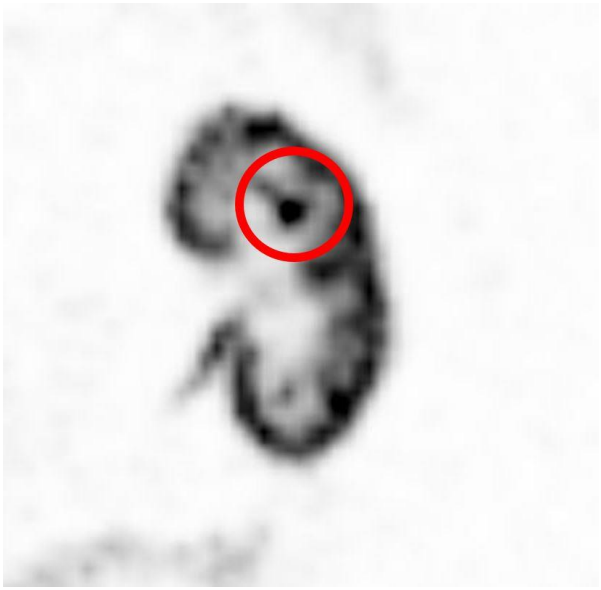

Figure-4

Example of strong asymmetry between kidneys: Due to mechanic outflow obstruction the right kidney (left on image) atrophied and later a nephrostomy was placed. PET (A), PET/CT (B) and ceCT (C).

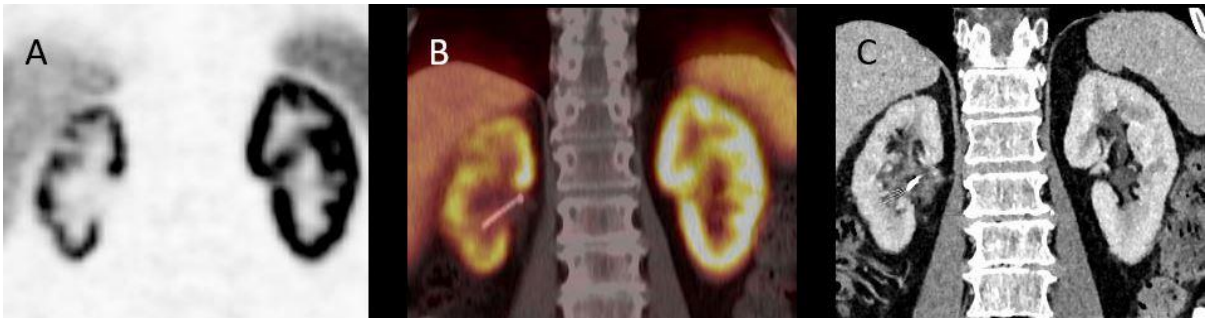

Graphical Abstract

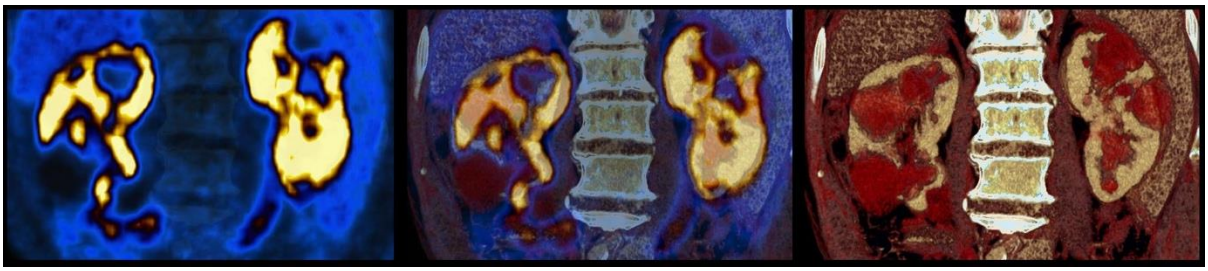

Table 1: Descriptive statistics for patients characteristics (n=25).

Covariates	n	Mean	SD	Min	Max
Age	25	71.6	9.84	34	82
Weight	25	88.4	13.72	68	116
Height	25	175.4	5.07	163	182
BMI	25	28.70	4.0	22.7	37.6
GFR	25	78.64	17.71	53	134
Creatinine	25	85.32	17.02	50	114

SD: Standard deviation

Table 2: Measured values for renal PSMA PET parameters (n=25).

Covariates	n	Mean	SD	Min	Max
mean SUV_{max}	25	57.75	20.68	21.90	100.95
mean SUV_{mean}	25	27.68	10.68	12.97	57.75
mean SUL_{max}	25	41.86	13.9	15.4	66.97
mean SUL_{mean}	25	18.19	4.59	9.12	25.8
SUV_{mean} liver	25	4.46	1.38	2.1	6.8
SUV_{mean} blood pool (bp)	25	1.16	0.32	0.5	1.70
SUV_{mean} spleen	25	6.13	2.42	2.8	11.4
renal SUV_{max} liver ratio	25	14.33	6.95	3.22	32.65
renal SUV_{max} bp ratio	25	53.61	22.94	19.91	100.95
renal SUV_{max} spleen ratio	25	10.99	6.21	2.55	28.84
renal SUV_{mean} liver ratio	25	6.94	3.89	1.91	19.48
renal SUV_{mean} bp ratio	25	26.17	13.03	9.43	57.75
renal SUV_{mean} spleen ratio	25	5.23	4.86	1.51	16.50
Sum Vol	25	354	93.61	194	567
Sum TLG	25	9968.8	5042.7	2520	26999
Sum TLG(SUL)	25	7758.4	4093.8	1772.3	19112.9
Sum counts	25	8077.5	3985.8	2176	17473

SD: Standard deviation

Table 3: Spearman rank correlation coefficient estimate between GFR and Creatinine with several covariates along with their confidence interval using bootstrapping with bias-corrected and accelerated method based on 2000 resamples.

Covariates	GFR Rho (PV) (95% CI)	Creatinine Rho (PV) (95% CI)
SUV_{mean} liver	-0.310 (0.132) (-0.634, 0.118)	0.218 (0.295) (-0.246, 0.606)
SUV_{mean} blood pool	**-0.415 (0.039) (-0.753, 0.064)**	0.346 **(0.090)** (-0.105, 0.723)
SUV_{mean} spleen	-0.130 (0.535) (-0.519, 0.285)	0.057 (0.786) (-0.423, 0.514)
mean SUV_{max}	0.199 (0.340) (-0.224, 0.596)	-0.226 (0.278) (-0.583, 0.161)
mean SUV_{mean}	0.317 (0.123) (-0.090, 0.645)	-0.329 (0.108) (-0.653, 0.063)
renal SUV_{max} liver ratio	**0.402 (0.046) (0.028, 0.706)**	**-0.364 (0.074) (-0.731, 0.124)**
renal SUV_{max} bp ratio	**0.471 (0.018) (0.115, 0.736)**	**-0.422 (0.036) (-0.738, 0.017)**
renal SUV_{max} spleen ratio	0.245 (0.237) (-0.160, 0.614)	-0.210 (0.314) (-0.631, 0.287)
renal SUV_{mean} liver ratio	**0.505 (0.010) (0.102, 0.786)**	**-0.451 (0.024) (-0.800, 0.041)**
renal SUV_{mean} bp ratio	**0.574 (0.003) (0.220, 0.832)**	**-0.515 (0.008) (-0.820, -0.075)**
renal SUV_{mean} spleen ratio	0.353 (0.083) (-0.075, 0.689)	-0.304 (0.140) (-0.708, 0.209)
Sum counts	0.124 (0.554) (-0.245, 0.467)	-0.159 (0.446) (-0.537, 0.269)
Sum Vol	-0.005 (0.982) (-0.391, 0.397)	-0.038 (0.856) (-0.398, 0.324)
Sum TLG	0.225 (0.280) (-0.166, 0.570)	-0.268 (0.195) (-0.617, 0.164)
Age	**-0.683 (0.001) (-0.907, -0.344)**	**0.565 (0.003) (0.175, 0.839)**
Weight	0.133 (0.528) (-0.224, 0.473)	-0.175 (0.402) (-0.530, 0.220)
Height	0.158 (0.452) (-0.279, 0.513)	-0.194 (0.354) (-0.546, 0.217)
BMI	0.061 (0.773) (-0.392, 0.466)	-0.100 (0.635) (-0.481, 0.341)
Mean SUL_{mean}	**0.343 (0.093) (-0.031, 0.622)**	-0.329 (0.108) (-0.640, 0.075)
Mean SUL_{max}	0.171 (0.413) (-0.229, 0.532)	-0.190 (0.362) (-0.555, 0.230)
Sum TLG(SUL)	0.334 (0.103) (-0.080, 0.644)	**-0.361 (0.076) (-0.653, 0.031)**

Rho: estimated Spearman rank correlation coefficient, PV: Probability value, CI: Confidence interval; PV are based on two sided test.